



Interaction potentials and ultracold scattering cross sections for the ${}^7\text{Li}^+ - {}^7\text{Li}$ ion-atom systemA. Pandey ,* M. Niranjan, N. Joshi , and S. A. Rangwala*Raman Research Institute, Light and Matter Physics, Sadashivanagar, Bangalore 560080, India*

R. Vexiau and O. Dulieu

Université Paris-Saclay, CNRS, Laboratoire Aimé Cotton, 91400 Orsay, France

(Received 27 June 2019; accepted 14 April 2020; published 11 May 2020)

We calculate the isotope-independent $\text{Li}^+ - \text{Li}$ potential energy curves for the electronic ground and first excited states. The scattering phase shifts and total scattering cross section for the ${}^7\text{Li}^+ - {}^7\text{Li}$ collision are calculated, with an emphasis on the ultralow-energy domain down to the s -wave regime. The effect of physically motivated alterations on the calculated potential energy curves is used to determine the bound of accuracy of the low-energy scattering parameters for the ion-atom system. It is found that the scattering length for the $A^2\Sigma_u^+$ state, $a_u = 1325a_0$, is positive and has well-constrained bounds. For the $X^2\Sigma_g^+$ state, the scattering length, $a_g = 20465a_0$, has a large magnitude, as it is sensitive to the restrained change of the potential, due to the presence of a vibrational state in the vicinity of the dissociation limit.

DOI: [10.1103/PhysRevA.101.052702](https://doi.org/10.1103/PhysRevA.101.052702)

I. INTRODUCTION

Experimental research on ion-atom interactions in dilute, trapped gas systems at ultracold temperatures is rapidly evolving towards detailed probes of the quantum dynamics of the resulting products [1–16]. One of the main goals is to thermalize an atomic ion within the ultracold atomic gas [2,3,5]. An atom and an ion mutually interact at a large internuclear distance, R , through an attractive charge-induced-dipole potential behaving as $\sim -\alpha_d/(2R^4)$, where α_d is the static dipole polarizability of the neutral atom. For energy $E \geq k_B \times 1$ mK, an ion-atom collision involves many partial waves ℓ , due to the strongly attractive long-range nature of their interaction [17], allowing a semiclassical description of the collision. Despite continuous progress regarding the precise control of the trapped ion motion, reaching the ultralow relative energy regime ($E/k_B \approx 1$ μK or lower) for ion-atom collisions is still challenging experimentally [4,6,18–20]. At these energies, quantum effects emerge, as few partial waves contribute to the collision. Due to ion heating as a result of interactions and trap imperfections in dynamical trapping, it is experimentally advantageous to investigate the full quantum regime at the highest possible temperatures [4,18].

The lowest possible centrifugal barrier is induced by the p wave ($\ell = 1$) and has a height equal to $1/(2\mu^2\alpha_d)$ (in atomic units of energy; a.u.). The p -wave barrier will be the highest for a low reduced mass, μ , thus opening the possibility of probing it at a relatively high collision energy. For this reason, lithium is implemented in several ongoing experiments [6,7,21,22]. Most hybrid ion-atom trapping experiments use an alkaline-earth ionic species suitable for laser cooling, which aids the achievement of low ion-atom collision

energies. The choice of a heteronuclear ion-atom combination, however, excludes the resonant charge exchange (RCE) mechanism, where an electron of the atom can be transferred to the ion without any energy release [1,8,9,23–26]. In our previous experiments [8,26], we have consistently exploited the RCE in the study of ion-atom collisions. We therefore focus this study on the scattering properties of ${}^7\text{Li}^+ - {}^7\text{Li}$, as this is a light system, with isotopic abundance, for going toward the quantum regime, with a p -wave barrier height of $k_B \times 2.98 \times 10^{-5}$ K.

In this paper, we perform calculations of the ${}^7\text{Li}^+ - {}^7\text{Li}$ interaction for the colliding ion and the atom when they are in their ground state. Specifically, in Sec. II we compute the *ab initio* potential energy curves (PECs) of $X^2\Sigma_g^+$, the electronic ground state, and $A^2\Sigma_u^+$, the first electronic excited state, of the Li_2^+ molecular ion using the multireference configuration interaction (MRCI) method and the best available basis sets. This is required despite the availability of previous high-quality calculations, since there is a significant discrepancy (factor of ≈ 2) between the calculations for a_g [27,28], the scattering length for the $X^2\Sigma_g^+$ state, which determines the low-energy ion-atom scattering cross section. These molecular ion *ab initio* PECs are smoothly matched to their physical asymptotic forms in the large- R range. We then derive the phase shifts characterizing the ${}^7\text{Li}^+ - {}^7\text{Li}$ collision as functions of the energy. The resulting scattering lengths a_g and a_u of the $X^2\Sigma_g^+$ and $A^2\Sigma_u^+$ states, respectively, are both computed to be positive with $a_g \gg a_u$. Our results are consistent with previous studies on the $X^2\Sigma_g^+$ and $A^2\Sigma_u^+$ PECs [27,29–35]. A convergence criterion is developed to bound the range of uncertainty within which the values of the scattering lengths, a_g and a_u , are constrained. The total cross sections obtained by computing the phase shifts are evaluated in Sec. III. We finally provide recommended values for the cross sections and their bounds for the ${}^7\text{Li}^+ - {}^7\text{Li}$ system in Sec. IV.

*amrendra.pandey@universite-paris-saclay.fr

TABLE I. Total electronic energies (in a.u.) of the $\text{Li}^+(^1S_0)$ and $\text{Li}(^2S_{1/2})$ ground states and their sum, $\text{Li}^+ + \text{Li}$, obtained from the present MRCI-SD calculations with increasing size of basis sets from aug-cc-pCVXZ, with $X \equiv \text{D, T, Q, 5}$. Another calculation using the coupled-cluster method, EA-EOM-CCSD, with ANO-RCC+ basis sets [33], is provided for comparison. Two separate calculations of Li^+ and Li representing the nonrelativistic variational calculations using Hylleraas coordinates are also listed [39,40].

$\text{Li}^+(^1S_0)$	$\text{Li}(^2S_{1/2})$	$\text{Li}^+ + \text{Li}$	Reference
-7.26922697	-7.46607917	-14.73530614	$X \equiv \text{D}$
-7.27690629	-7.47457432	-14.75148061	$X \equiv \text{T}$
-7.27870222	-7.47670230	-14.75540452	$X \equiv \text{Q}$
-7.27933195	-7.47740563	-14.75673758	$X \equiv 5$
-7.275561	-7.473553	-14.74911400	[33]
-7.27991339 ^a	-7.47806032310 ^b	-14.7579737131	[39], ^a [40] ^b

^a Li^+ .

^b Li .

II. Li_2^+ POTENTIAL ENERGY CURVES

A. *Ab initio* Born-Oppenheimer potentials

We compute the $X^2\Sigma_g^+$ and $A^2\Sigma_u^+$ states of Li_2^+ under the Born-Oppenheimer approximation using the MOLPRO package [36]. The complete active-space self-consistent field (CASSCF) and multireference configuration interaction with single and double excitation (-SD) methods are used. Full-valence-type CASSCF wave functions, which consider all five electrons of Li_2^+ as active, are calculated and used as the reference functions for the MRCI calculations [37]. We choose this approach as it is variational for the truncated configuration interaction expansion, to ensure convergence towards the true energies for both states with the basis-set size. The reference calculations are performed with the largest available basis set, namely, the augmented Dunning correlation-consistent, polarized valence, 5-zeta basis set, aug-cc-pCV5Z [38].

Due to the large discrepancies between a_g values reported in the literature [27,28], we determine bounds for a_g so that more precise calculations in the future should not supersede the conclusions drawn here. We first compute the atomic energies of Li and Li^+ in their ground state (Table I). Various sizes of the aug-cc-pCVXZ basis sets are considered, with $X \equiv \text{D}$ (double), T (triple), Q (quadruple), and 5 (quintuple) referring to the largest excitation degree of the determinants.

This allowed us to reach a relative convergence of better than 0.009%. Our variational values are larger in magnitude by 0.05% than those obtained in [33] using a coupled-cluster approach with single and double excitations (CCSD) and the ANO-RCC+ basis set. As Li^+ and Li are small systems, with two and three electrons, respectively, extremely precise atomic calculations can be performed. Our energies obtained with the aug-cc-pCV5Z basis set differ by only 0.008% from the best available variational calculations using Hylleraas coordinates [39,40] (Table I), justifying the choice of the aug-cc-pCV5Z set as an appropriate one for molecular calculations.

The sum of the electronic energies of $\text{Li}^+(^1S_0)$ and $\text{Li}(^2S_{1/2})$, from Table I and the energy of the dissociation limit obtained from the molecular calculation, E_∞ (Table II), exhibit a small difference (0.004 cm^{-1}), which is assigned to the basis-set superposition error. We calculated this effect for the Li atom, using the effective core potential and core polarization potential with one valence electron (see the method labeled Th_2 further on). The basis-set superposition error amounts to less than 0.2 cm^{-1} at the equilibrium distance, R_e , and to 0.006 cm^{-1} at $R = 50a_0$ (a_0 is the Bohr radius). Hence for the scattering calculation this correction is not incorporated into the potentials.

In order to provide a convergence criterion on potential energies, we compute the *ab initio* $X^2\Sigma_g^+$ and $A^2\Sigma_u^+$ PECs with a series of aug-cc-pCVXZ basis sets (with $X \equiv \text{D, T, Q, 5}$) in the $[2a_0-50a_0]$ internuclear distance range, with a $0.2a_0$ step. They correlate with the lowest asymptotic limit $\text{Li}^+(^1S_0) + \text{Li}(^2S_{1/2})$. We report in Table II the total potential energy E_∞ for $R \rightarrow \infty$, i.e., at the dissociation limit (see Sec. II B), and E_e at the equilibrium distance, R_e , the well depth, $D_e = E_\infty - E_e$, and the position of the repulsive wall, R_{in} , at the well depth. The relative changes ΔE_∞ and ΔE_e of E_∞ and E_e with increasing size of the basis set are also reported. Their progressions show a convergence similar to that observed for $\text{Li}^+(^1S_0) + \text{Li}(^2S_{1/2})$ (Table I). The energy of $\text{Li}^+(^1S_0) + \text{Li}(^2S_{1/2})$ in the complete-basis-set limit is the best variational representation of the dissociation limit, E_∞ , and should ideally be attained in the full configuration interaction (FCI) and complete-basis-set limit of the $\text{Li}_2^+ X^2\Sigma_g^+$ and $A^2\Sigma_u^+$ PECs. The difference between $\text{Li}^+(^1S_0) + \text{Li}(^2S_{1/2})$ obtained from the best available atomic calculation, listed in Table I [39,40], and the E_∞ obtained from the aug-cc-pCV5Z

TABLE II. Dissociation limit, E_∞ , its convergence with basis sets, ΔE_∞ , total energy E_e at R_e , its convergence with basis sets, ΔE_e , equilibrium distance, R_e , well depth, D_e , and repulsive wall position R_{in} of the $X^2\Sigma_g^+$ and $A^2\Sigma_u^+$ PECs of $^7\text{Li}_2^+$. Results for various basis sets aug-cc-pCVXZ, with $X \equiv \text{D, T, Q, 5}$, are listed.

Electronic state	E_∞ (a.u.)	ΔE_∞ (%)	E_e (a.u.)	ΔE_e (%)	R_e (units of a_0)	D_e (cm^{-1})	R_{in} (units of a_0)	aug-cc-pCVXZ basis sets, with $X \equiv$
$X^2\Sigma_g^+$	-14.73530934		-14.78224306		5.940	10 300.76	3.758	D
	-14.75148110	0.1097	-14.79891577	0.1128	5.875	10 410.70	3.723	T
	-14.75540520	0.0266	-14.80300996	0.0277	5.865	10 448.03	3.715	Q
	-14.75673756	0.0090	-14.80438625	0.0093	5.858	10 458.58	3.713	5
$A^2\Sigma_u^+$	-14.73530934		-14.73570944		18.939	87.81	15.630	D
	-14.75148110	0.1097	-14.75188381	0.1098	18.839	88.38	15.563	T
	-14.75540520	0.0266	-14.75580764	0.0266	18.818	88.32	15.545	Q
	-14.75673756	0.0090	-14.75714022	0.0090	18.799	88.37	15.540	5

TABLE III. Fundamental spectroscopic constants of the $X^2\Sigma_g^+$ and $A^2\Sigma_u^+$ PECs for ${}^7\text{Li}_2^+$. Exp refers to the best available experimental determination, while the numbered Th labels refer to various theoretical determinations.

State and method, $X^2\Sigma_g^+/A^2\Sigma_u^+$	R_e (units of a_0)	D_e (cm^{-1})	ω_e (cm^{-1})	$\omega_e x_e$ (cm^{-1})	B_e (cm^{-1})	Ref. No.
X						
Exp	5.88	$10\,464 \pm 6$	262.2 ± 1.5	1.7 ± 0.5	0.496 ± 0.002	[47,48]
Th ₁	5.858	10 458.58	261.96	1.51	0.500	Present study
Th ₂	5.838	10 515.76	262.54	1.50	0.503	Present study
Th ₃	5.863	10 439	262.58	1.58	—	[33]
Th ₄	5.877	10 457.7	261.6	1.47	—	[27]
Th ₅	5.844	10 498	263.39	—	—	[32]
Th ₆	5.848	10 475	264	1.94	0.506	[31]
Th ₇	5.856	10 441	263.76	1.646	0.5006	[29]
Th ₈	5.826	10 494	262.771	1.645	0.505	[34]
Th ₉	5.899	10 466	263.08	1.477	0.4945	[30]
Th ₁₀	5.877	10 457	266.2	—	0.4753	[35]
A						
Th ₁	18.799	88.37	16.15	0.84	0.0486	Present study
Th ₂	18.797	88.71	16.17	0.84	0.0486	Present study
Th ₃	18.795	88	15.98	0.81	—	[33]
Th ₄	18.798	88.4	16.63	1.05	—	[27]
Th ₅	18.787	89	15.92	—	—	[32]
Th ₆	18.729	88	15.81	0.74	0.049	[31]
Th ₇	18.802	90	20.1	0.13	0.049	[29]
Th ₈	18.763	89	16.312	0.750	0.0487	[34]
Th ₉	18.899	90	16.01	0.79	0.049	[30]

calculation, listed in Table II, is smaller than the difference in the E_∞ values obtained from the two cases $X \equiv Q$ and $X \equiv 5$, suggesting a good convergence. The observed bound on E_∞ suggests that molecular calculations of the Li_2^+ in the FCI and complete-basis-set limits will not result in a change in the well depth, D_e , of $X^2\Sigma_g^+$ more than 10 cm^{-1} larger (i.e., the difference between the D_e' values obtained in the $X \equiv Q$ and $X \equiv 5$ cases) than the value obtained with the aug-cc-pCV5Z basis set. The experimental value of D_e (Table III) also supports the above theoretical bound.

The *ab initio* $X^2\Sigma_g^+$ and $A^2\Sigma_u^+$ PECs, hereafter denoted V_g^{ab} and V_u^{ab} , respectively, relative to E_∞ are shown in Fig. 1 [41]. The lower inset displays the difference between these PECs and those obtained from the method in [42] based on the representation of the Li^+ cores by an effective core potential (ECP) and a core polarization potential (CPP) (referred to as the Th₂ method), thus treating the Li_2^+ molecule as a one-electron system (see also, for instance, [30]). The overall agreement is satisfactory between the two approaches, with the largest difference in energy at $12a_0$ about 1%. Below $6a_0$, the difference is much larger, which can be understood to indicate that the ECP + CPP approach restrains the calculation from precisely representing the core-valence correlation at short internuclear distances.

B. Determination of asymptotic extensions of PECs

The low-energy scattering wave functions need to be computed up to large internuclear distances, with $R \gg \lambda$, where λ is the de Broglie wavelength of the colliding system (for ${}^7\text{Li}^+ - {}^7\text{Li}$, $10a_0 < \lambda < 10^6a_0$ for collision energies $10^{-5} \text{ a.u.} > E > 10^{-15} \text{ a.u.}$). The *ab initio* PECs, in the

large- R limit, generally become less accurate, as the molecular orbitals which are built during the calculations are not best adapted to the situation of separated atoms. Instead, we use the well-established asymptotic functional form $V_p^a(R)$ derived from the multipolar expansion of the interaction energy in

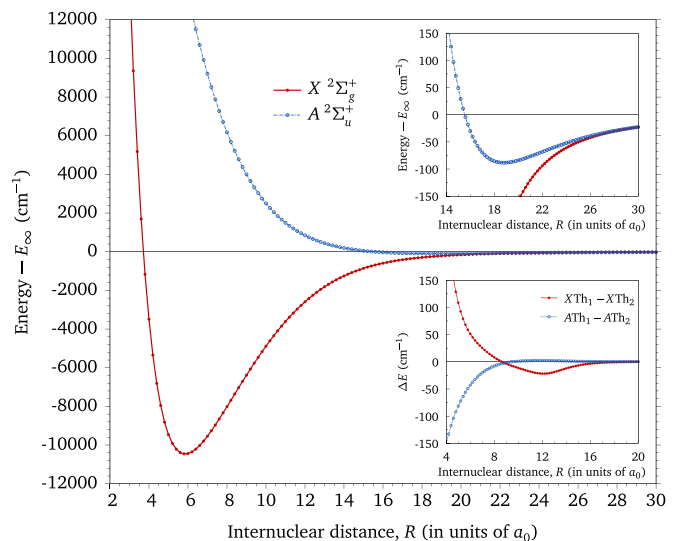


FIG. 1. ${}^7\text{Li}_2^+$ potential energy curves $X^2\Sigma_g^+$ and $A^2\Sigma_u^+$, computed in the present work (MRCI-SD with the aug-cc-pCV5Z basis set), and denoted XTh₁ and ATh₁, respectively. Upper inset: Minima of the $A^2\Sigma_u^+$ curve. Lower inset: Energy differences ΔE with the curves calculated using the approach in [42] (denoted XTh₂ and ATh₂). The corresponding spectroscopic constants are listed in Table II.

inverse powers of R ,

$$V_p^a(R) = V_{\text{ind}}^a(R) \mp V_{\text{exch}}^a(R), \quad p \equiv \{g, u\}, \quad (1)$$

where g (u) corresponds to $X^2\Sigma_g^+$ ($A^2\Sigma_u^+$). The asymptotic induction term $V_{\text{ind}}^a(R)$ is expressed as [43]

$$V_{\text{ind}}^a(R) = -\left[\frac{C_4}{R^4} + \frac{C_6}{R^6} + \frac{C_8}{R^8} + \dots\right], \quad (2)$$

where $C_4 = \alpha_d/2$, $C_6 = \alpha_q/2$, and $C_8 = \alpha_o/2$, with α_d , α_q , and α_o being the dipole, quadrupole, and octupole static polarizabilities of the ${}^7\text{Li}$ ground-state atom. We take the values from Tang *et al.* [44,45]: $\alpha_d = 164.161$ a.u., $\alpha_q = 1423.415$ a.u., and $\alpha_o = 39\,653.720$ a.u. The van der Waals (dispersion) interaction, also varying as $1/R^6$, which is generally small for ion-atom cases [27,43], will be included in an effective manner in the potential finally used in the scattering calculations.

The asymptotic exchange term reads [46]

$$V_{\text{exch}}^a(R) = \frac{1}{2}AR^\alpha e^{-\beta R} \left[1 + \frac{B}{R} + \frac{C}{R^2} + \dots\right], \quad (3)$$

where the parameters $\alpha = 2.1774$ a.u., $\beta = 0.6294$ a.u., and $B = 0.5191$ a.u. are simple functions of the ${}^7\text{Li}$ ionization energy [43,46]. The A and C parameters are obtained from the fits of the *ab initio* exchange energy, $V_{\text{exch}}^{\text{ab}}$, given by half the difference of the *ab initio* $A^2\Sigma_u^+$ (V_u^{ab}) and $X^2\Sigma_g^+$ (V_g^{ab}) PECs with Eq. (3). The interval $23a_0 < R < 28a_0$ is used in the fitting procedure, yielding $A = 0.133\,899$ a.u. and $C = 27.7397$ a.u. The selected interval gives us the fit with the smallest relative residuals. The same A and C provide an excellent fit for the entire range above $R > 28a_0$. This suggests that for the exchange energy, the selected range represents the asymptotic limit, and it fixes the functional form of the exchange energy for ${}^7\text{Li}_2^+$, i.e., $V_{\text{exch}}^c(R)$. The *ab initio* exchange energy, $V_{\text{exch}}^{\text{ab}}$, intersects the function $V_{\text{exch}}^c(R)$ at $R = 25.6a_0$, which is selected as the point beyond which asymptotic expansions are used. $V_{\text{exch}}^a(R)$ [or $V_{\text{exch}}^c(R)$] decays exponentially with R , so in the large- R limit, only the contribution of $V_{\text{ind}}^a(R)$ remains significant. Around $35a_0$, $V_{\text{exch}}^a(R)$ becomes smaller than 0.1% of $V_{\text{ind}}^a(R)$. Moreover, the contributions of the C_6/R^6 and C_8/R^8 terms become smaller than 1% of the induction energy beyond $29.5a_0$ and $12.5a_0$, respectively. In the internuclear range where only the C_4/R^4 term contributes significantly, E_∞ is obtained using a fit to the *ab initio* induction energy, given by the average of the $A^2\Sigma_u^+$ (V_u^{ab}) and $X^2\Sigma_g^+$ (V_g^{ab}) PECs, with the form given in Eq. (2) using C_6 as a free parameter in the range $35a_0$ – $50a_0$. For a calculation with the aug-cc-pCV5Z basis set, the change in E_∞ for different fit ranges, varying from $25a_0$ – $50a_0$ to $35a_0$ – $50a_0$, is only ~ 0.02 cm $^{-1}$.

After setting E_∞ as the origin of energies of the PECs, calculation of the extension of potentials for large R is performed under the following conditions: (i) the PECs $X^2\Sigma_g^+$ and $A^2\Sigma_u^+$ used in the scattering calculations and their derivatives are kept continuous at $R = 25.6a_0$, and (ii) the PECs approach $V_p^a(R)$ as $R \rightarrow \infty$. First, an R -dependent coefficient, $C_4(R)$, is determined by expressing the *ab initio* PECs in the range $20a_0 < R < 50a_0$ as

$$V_p^{\text{ab}} = V_{\text{ind}}^c(R) \mp V_{\text{exch}}^c(R), \quad (4)$$

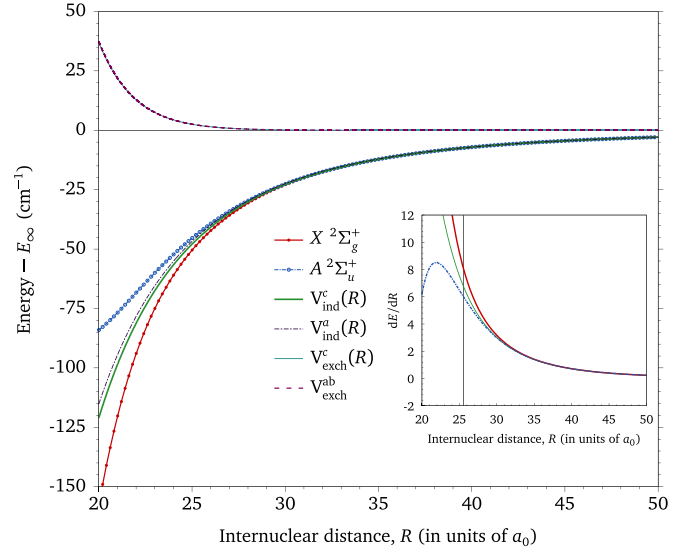


FIG. 2. Asymptotically extended PECs $X^2\Sigma_g^+$ (solid red line) and $A^2\Sigma_u^+$ (solid blue line) of ${}^7\text{Li}_2^+$. The asymptotic induction function and *ab initio* exchange term, $V_{\text{ind}}^a(R)$ and $V_{\text{exch}}^{\text{ab}}$, and the computed induction and exchange functions, $V_{\text{ind}}^c(R)$ and $V_{\text{exch}}^c(R)$, are plotted for comparison. Inset: First derivatives of the $X^2\Sigma_g^+$ and $A^2\Sigma_u^+$ PECs and $V_{\text{ind}}^c(R)$.

with

$$V_{\text{ind}}^c(R) = -\left[\frac{C_4(R)}{R^4} + \frac{C_6}{R^6} + \frac{C_8}{R^8}\right], \quad (5)$$

and the functional form of $V_{\text{exch}}^c(R)$, which is determined previously. Then, from the computed $C_4(R)$, the functional forms of $\partial C_4/\partial R$ and $C_4(R)$ and, consequently, of $V_{\text{ind}}^c(R)$ are obtained. In this way, the small van der Waals term is included in the function $V_{\text{ind}}^c(R)$ in an effective way. The final scattering potentials $X^2\Sigma_g^+$ and $A^2\Sigma_u^+$, denoted $V_p^c(R)$, use *ab initio* values for $R < 25.6a_0$ and $V_{\text{ind}}^c(R) \mp V_{\text{exch}}^c(R)$ for $R > 25.6a_0$.

The asymptotically extended PECs, $X^2\Sigma_g^+$ and $A^2\Sigma_u^+$, $V_p^c(R)$ [41], the asymptotic induction function and *ab initio* exchange energy, $V_{\text{ind}}^a(R)$ and $V_{\text{exch}}^{\text{ab}}$, and the computed induction and exchange functions, $V_{\text{ind}}^c(R)$ and $V_{\text{exch}}^c(R)$, are shown in Fig. 2. The difference between $V_{\text{ind}}^a(R)$, which uses a constant C_4 , and $V_{\text{ind}}^c(R)$, which uses a derived R -dependent function $C_4(R)$, is quite evident in the $20a_0$ – $25a_0$ range (see Fig. 2). This procedure fixes in a consistent way the asymptotic form of the PECs for reliable scattering calculations at extremely low energies.

C. Criterion for bounds on the scattering parameters

The previous section demonstrates that the asymptotic ion-atom interaction is well determined by the highly accurate calculations. Therefore the large variation in the low-energy ion-atom cross sections reported in the literature is illustrative of their strong sensitivity to the *ab initio* part of the PECs, given that the small- R region of the potentials is strongly influenced by the growing contribution of the core electrons and thus is represented least accurately. To estimate the effect of this dependence on the scattering parameters, a set of PECs for $X^2\Sigma_g^+$ and $A^2\Sigma_u^+$ is generated by continuously varying

the potentials according to

$$R^p = R + r_p(R - R_e)/(R_{\text{in}} - R_e) \quad \forall R < R_e, \quad (6)$$

where R^p denotes the coordinate of the generated PECs, and r_p is the change in the repulsive wall position R_{in} . The allowed variation in the small- R region (i.e., $R < R_e$) of the potentials is estimated by comparing the D_e from the PECs obtained using different methods and basis sets (Table III) with our values computed with basis sets aug-cc-pCVXZ with $X \equiv \text{D, T, Q, 5}$ (Table II). The difference in the well depths for the $X^2\Sigma_g^+$ obtained from aug-cc-pCVTZ and aug-cc-pCV5Z covers a similar variation, $\approx 40 \text{ cm}^{-1}$, as observed from XTh₁₋₉ and X_{Exp} (Table III). The difference between the repulsive wall of PECs computed using the aug-cc-pCV5Z and aug-cc-pCVTZ basis sets is thus taken as the permissible range of change in the wall positions of the PEC models with $\Delta R = \pm r_p$, $p \equiv \{g, u\}$, with $r_g = 0.01a_0$ for $X^2\Sigma_g^+$ and $r_u = 0.02a_0$ for $A^2\Sigma_u^+$. The determined energy bound for the allowed change in the small R is much larger than the contributions arising from relativistic effects, the diagonal Born-Oppenheimer correction, and other corrections. A comparison is provided in Sec. IV. The sets of PECs are created using the linear scaling of Eq. (6) for the required change in $\Delta R = \pm r_p$, $p \equiv \{g, u\}$, at the repulsive wall position R_{in} . The scattering calculations are performed for the two limiting modifications to both the $X^2\Sigma_g^+$ and the $A^2\Sigma_u^+$ curves with suffixes “: $\Delta R = \pm r_{g/u}$ ” and for the *ab initio* curves denoted “: $\Delta R = 0$ ”.

An extensive comparison of the present results for the states obtained with the aug-cc-pCV5Z basis set, $X^2\Sigma_g^+:\Delta R = 0$ and $A^2\Sigma_u^+:\Delta R = 0$ (referred to as Th₁), with those previously published in the literature is presented in Table III. The vibrational levels of the $X^2\Sigma_g^+:\Delta R = 0$ and $A^2\Sigma_u^+:\Delta R = 0$ curves are evaluated using the LEVEL numerical code [49]. The $X^2\Sigma_g^+$ ($A^2\Sigma_u^+$) PEC supports 82 (16) vibrational levels with vibrational harmonic constant $\omega_e = 261.96 \text{ cm}^{-1}$ and anharmonicity constant $\omega_e x_e = 1.51 \text{ cm}^{-1}$ ($\omega_e = 16.15 \text{ cm}^{-1}$ and $\omega_e x_e = 0.84 \text{ cm}^{-1}$). The overall shape of the bottom of the potential curve, described by ω_e , $\omega_e x_e$, and B_e , is well reproduced by all calculations. They are in good agreement with the best available results from optical-optical double resonance spectroscopy [47,48], falling within the reported error bars. We see that the present approach (Th₁) and the simpler method (Th₂), mentioned in Sec. II. A, are in remarkable agreement (about 0.5% for the equilibrium distance R_e , the well depth D_e , and the rotational constant B_e and even 0.2% for the vibrational constant ω_e).

Up to now the calculations have been performed with the core-optimized basis set and the active core; i.e., core excitations are included. To assess the contribution of the core electrons, we have performed an additional set of MRCI calculations with cc-pVXZ; $X \equiv \text{D, T, Q, 5}$, which are the basis sets self-consistently produced from the atomic calculations with the frozen-core electrons. The cc-pVXZ; $X \equiv \text{D, T, Q, 5}$ basis sets are similar to the aug-cc-pCVXZ; $X \equiv \text{D, T, Q, 5}$ sets, the core-optimized basis with an augmented function, used in this work. PECs computed with cc-pVXZ; $X \equiv \text{D, T, Q, 5}$ are mostly similar to their respective aug-cc-pCVXZ; $X \equiv \text{D, T, Q, 5}$ PECs in the large- R region but are significantly inaccurate in the small- R region (especially $R < R_e$). These

calculations show that the repulsive wall positions of the PECs obtained from the frozen-core basis sets erroneously fall below the repulsive walls of the respective PECs with the active-core basis sets. In the case of frozen-core basis sets and frozen-core calculations, the unoptimized core continues to retain higher electron densities between the two nuclei than in cases where they are energy optimized along with the valence electrons. It, consequently, pushes the repulsive wall to lower values of R , much beyond the convergence limit shown in Figs. 3(c) and 3(d). We find that, for small electronic systems, it is essential that PEC calculations are performed with core-optimized basis sets in which all electrons of the molecular system are variationally optimized.

III. ${}^7\text{Li}^+ - {}^7\text{Li}$ COLLISION CROSS SECTIONS

Applying standard scattering theory based on the partial-wave expansion of the total wave function in R , the Schrödinger equation for a single partial wave, ℓ , at a collision energy $E = \hbar^2 k^2/(2\mu)$, $k = 2\pi/\lambda$ is

$$\left[-\frac{\hbar^2}{2\mu} \frac{d^2}{dR^2} + \frac{\hbar^2}{2\mu} \frac{\ell(\ell+1)}{R^2} + V_p^c(R) \right] y_p^{E,\ell}(R) = E y_p^{E,\ell}(R), \quad (7)$$

where μ is the (${}^7\text{Li}^+ - {}^7\text{Li}$) Watson's charge-modified reduced mass [50]. The asymptotic form of the wave function $y_p^{E,\ell}(R)$ is given by $y_p^{E,\ell}(R) \simeq kR[j_\ell(kR)\cos(\eta_p^\ell) - n_\ell(kR)\sin(\eta_p^\ell)]$, where $j_\ell(kR)$ and $n_\ell(kR)$ are the spherical Bessel functions, and η_p^ℓ is the quantum phase shift generated by the scattering potential $V_p^c(R)$. Equation (7) is solved numerically, and η_p^ℓ is extracted at large distances, namely, at $R = 10\lambda$, as the asymptotic limit for low energies when $\lambda > 100a_0$ and at $R = 1000a_0$ for higher energies when $\lambda < 100a_0$.

In Fig. 4, the quantum phase shifts η_p^ℓ (modulo π) are shown for $E = 10^{-5}$ a.u. (or $\sim 2 \text{ cm}^{-1}$) and $E = 10^{-6}$ a.u. (or $\sim 0.2 \text{ cm}^{-1}$). For large ℓ , when the outer classical turning point at a given collision energy is such that $V_p^c(R)$ can be approximated to the leading term $-\alpha_d/2R^4$ of $V_{\text{ind}}^a(R)$, one can define the semiclassical phase shift as $\eta_{\text{sc}}^\ell \approx (\pi\mu^2\alpha_d)/(4\hbar^4) \times E/\ell^3$ and thus the semiclassical cross section is $\sigma_{\text{sc}}(E) = \pi(\mu\alpha_d^2/\hbar^2)^{1/3}(1 + \pi^2/16) \times E^{-1/3}$ [24]. The semiclassical phase shifts are in agreement with the quantum phase shifts for $\ell > L_{\text{sc}}$, with $L_{\text{sc}} = 41$ for $E = 10^{-5}$ a.u. and $L_{\text{sc}} = 19$ for $E = 10^{-6}$ a.u. Around $E = 10^{-8}$ a.u. (or $\sim 0.002 \text{ cm}^{-1}$), as the contribution to the cross section from partial waves $\ell > 10$ becomes negligible, resonance features arise.

In Fig. 5, the quantum phase shifts η_g^ℓ for $\ell = 0, 1$ are plotted as a function of the collision energy for the *ab initio* PEC, $X^2\Sigma_g^+:\Delta R = 0$, and the generated PECs with shifted repulsive walls, $X^2\Sigma_g^+:\Delta R = \pm r_g$. At low energies, the effect is weak for $\ell > 0$, as the centrifugal barrier becomes dominant in the collision. Note that the s -wave ($\ell = 0$) phase shift changes sign when the repulsive wall is slightly shifted, indicating the presence of a pole where the scattering length diverges. As a result, the accuracy of the PEC becomes a major factor in determining the collision cross section. This is the primary motivation for the extreme care taken in determining the scattering potential in Sec. II.

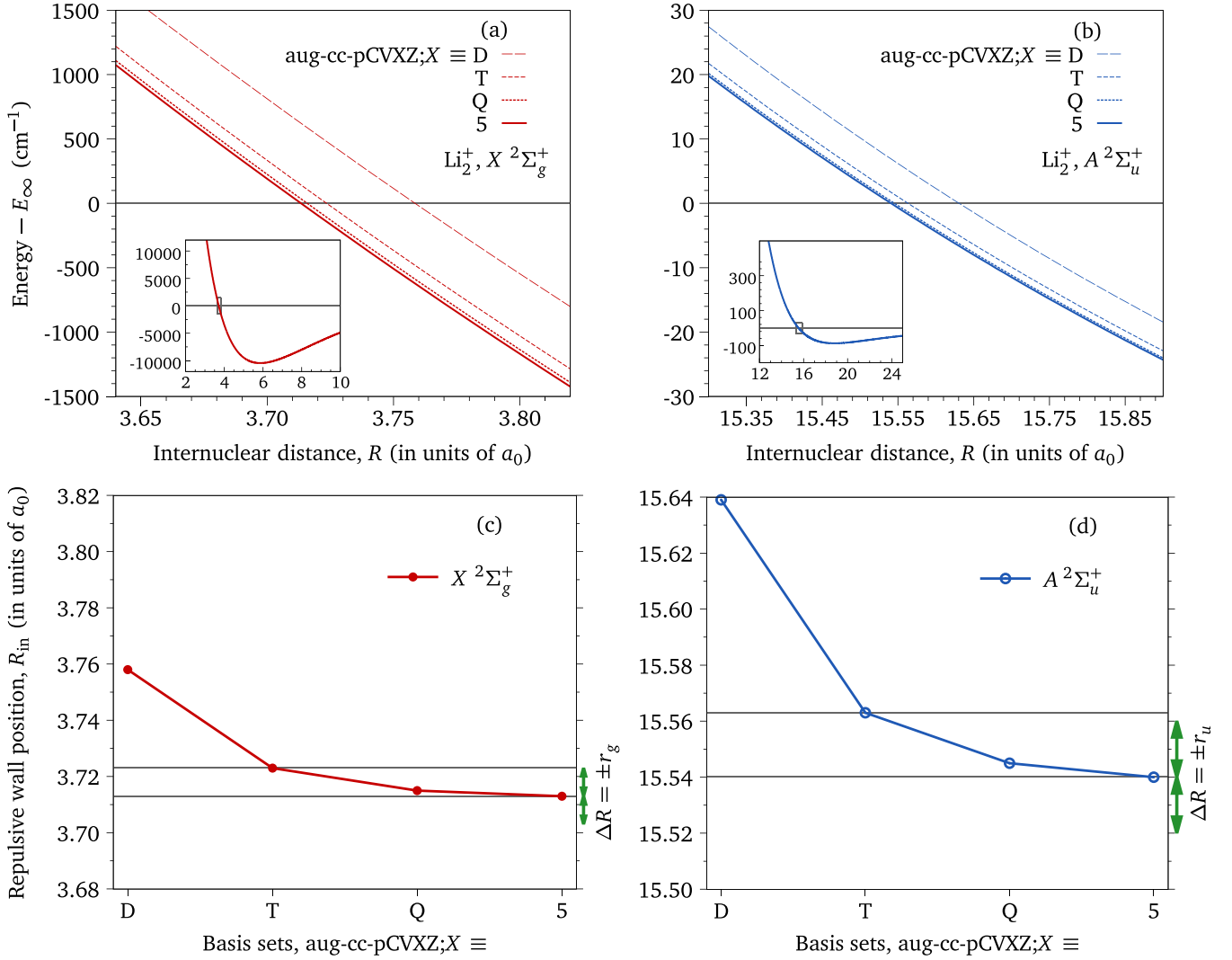


FIG. 3. Potential energy curves near the repulsive wall (see insets) for $X^2\Sigma_g^+$ (a) and $A^2\Sigma_u^+$ (b), computed using the basis sets aug-cc-pCVXZ with $X \equiv D, T, Q, 5$, and corresponding positions R_{in} of their inner turning points at the dissociation limit E_∞ (c, d). Selected ranges ΔR for the variation of the repulsive wall of the aug-cc-pCV5Z calculations mimicking possible inaccuracies in cross-section calculations are shown: $\Delta R = \pm r_{g/u}$ with $r_g = 0.01a_0$ and $r_u = 0.02a_0$ for $X^2\Sigma_g^+$ and $A^2\Sigma_u^+$, respectively.

Due to the identical nuclei, the scattering between the ${}^7\text{Li}^+ - {}^7\text{Li}$ ion-atom system enables the event in which the ion and the atom exchange their charge identities. A scattering event when the initial identities are preserved is a direct elastic collision, whereas an event where the identities of the ion-atom pair are interchanged is termed a resonant charge exchange collision [17]. The scattering amplitudes for direct elastic and RCE collisions are given by $(f_g + f_u)/2$ and $f_{ce} = (f_g - f_u)/2$, where f_g and f_u are the scattering amplitudes for $X^2\Sigma_g^+$ and $A^2\Sigma_u^+$. We define $S_g(E)$ and $S_u(E)$ in Eq. (8) and $S_{ce}(E)$ in Eq. (9), where $d\Omega$ is the differential solid angle, as

$$S_p(E) = \int |f_p|^2 d\Omega = \frac{4\pi}{k^2} \sum_{\ell=0}^{\infty} (2\ell + 1) \sin^2(\eta_p^\ell), \quad (8)$$

$$S_{ce}(E) = \int |f_{ce}|^2 d\Omega = \frac{\pi}{k^2} \sum_{\ell=0}^{\infty} (2\ell + 1) \sin^2(\eta_g^\ell - \eta_u^\ell). \quad (9)$$

The average $(S_g(E) + S_u(E))/2$ has been identified as the total cross section, and $S_{ce}(E)$ as the RCE cross section when certain approximations are made [43] at high collision energies. The functions $S_g(E)$ and $S_u(E)$ for the ${}^7\text{Li}^+ - {}^7\text{Li}$ system as functions of the collision energy are shown along with the semiclassical scattering cross section, $\sigma_{sc}(E)$, in Figs. 6(a) and 6(b). For ${}^7\text{Li}^+ - {}^7\text{Li}$, $\sigma_{sc}(E) = 2826 \times E^{-1/3}$ a.u. The Langevin cross section, $\sim \pi(2\alpha_d)^{1/2} \times E^{-1/2}$, for ${}^7\text{Li}^+ - {}^7\text{Li}$, $56.92 \times E^{-1/2}$ a.u., and Langevin/4 are shown along with $S_{ce}(E)$ in Fig. 6(c). In all cases, the cross sections include the sum of the first 100 partial waves. It can be seen that $S_{ce}(E)$, in this case, predominantly falls in the range defined by Langevin and Langevin/4. For low energies, $S_{ce}(E)$ varies significantly from the expected semiclassical picture.

For homonuclear systems, in principle, individual scattering channels cannot be measured independently and therefore we compute the total cross section $\sigma_{tot}(E)$, given in Eq. (10). The expression for $\sigma_{tot}(E)$ differs from the one usually

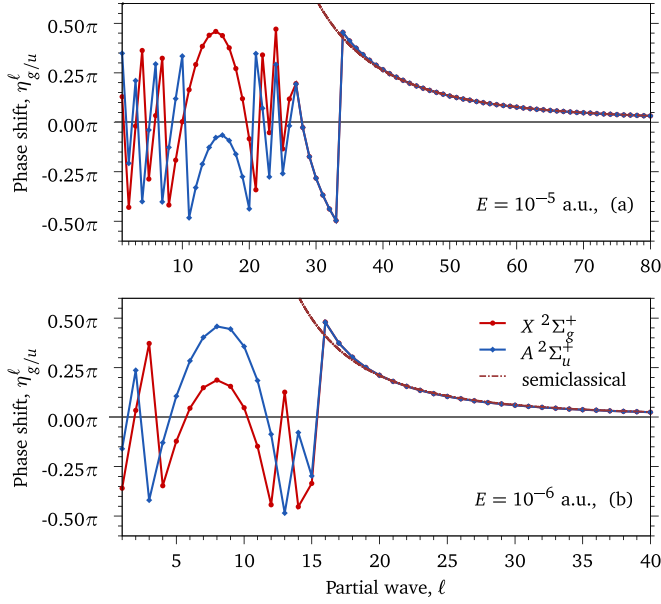


FIG. 4. Quantum (modulo π) and semiclassical phase shifts as functions of the partial waves, ℓ , for a collision along the $X^2\Sigma_g^+:\Delta R = 0$ and $A^2\Sigma_u^+:\Delta R = 0$ curves for the collision energies 10^{-5} a.u. (a) and 10^{-6} a.u. (b). Lines joining the points are a guide for the eye.

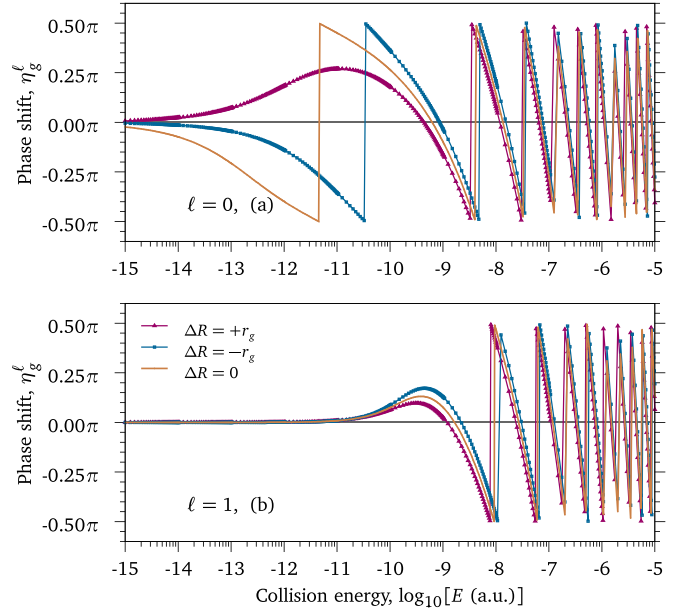


FIG. 5. Quantum phase shift (modulo π) of the $X^2\Sigma_g^+:\Delta R = \pm r_g$ and *ab initio* $X^2\Sigma_g^+:\Delta R = 0$ curves as a function of the collision energy for the partial waves $\ell = 0$ (a) and $\ell = 1$ (b). At low energies, the change in the phase shifts for different PEC models are significant only for $\ell = 0$.

employed in the literature; the derivation will be discussed elsewhere [51]:

$$\sigma_{\text{tot}}(E) = \frac{4\pi}{k^2} \left[x \left[\sum_{\text{even}} (2\ell + 1) \sin^2(\eta_g^\ell) \right] + \sum_{\text{odd}} (2\ell + 1) \sin^2(\eta_u^\ell) \right]$$

$$+ (1-x) \left[\sum_{\text{odd}} (2\ell + 1) \sin^2(\eta_g^\ell) + \sum_{\text{even}} (2\ell + 1) \sin^2(\eta_u^\ell) \right], \quad (10)$$

where x is a function of the nuclear spin I . For a half-integer nuclear spin, $x = I/(2I + 1)$. For ${}^7\text{Li}$, with $I = 3/2$, x is $3/8$ [43]. The cross section evaluated using Eq. (10) differs

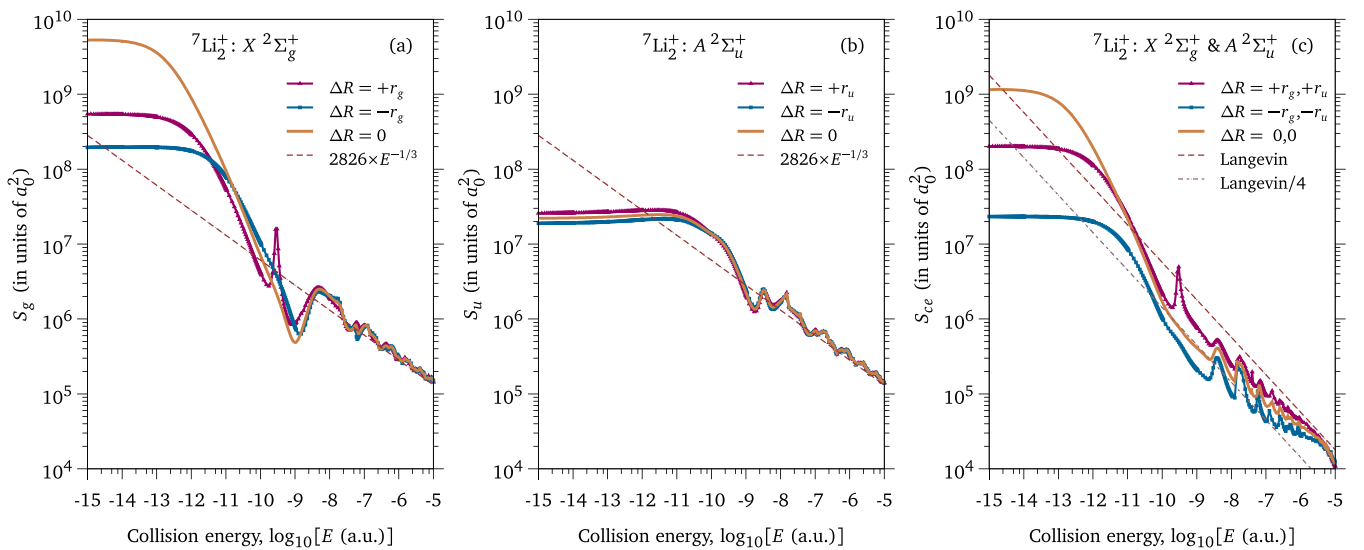


FIG. 6. (a) $S_g(E)$ for the generated $X^2\Sigma_g^+:\Delta R = \pm r_g$ and $X^2\Sigma_g^+:\Delta R = 0$ curves. (b) $S_u(E)$ for $A^2\Sigma_u^+:\Delta R = \pm r_u$ and $A^2\Sigma_u^+:\Delta R = 0$. In (a) and (b), the semiclassical cross section, $2826 \times E^{-1/3}$, is shown. (c) $S_{cc}(E)$ for the two bounding modifications of PECs, $X^2\Sigma_g^+:\Delta R = +r_g$, $A^2\Sigma_u^+:\Delta R = +r_u$ and $X^2\Sigma_g^+:\Delta R = -r_g$, $A^2\Sigma_u^+:\Delta R = -r_u$, along with $S_{cc}(E)$ for the $X^2\Sigma_g^+:\Delta R = 0$, $A^2\Sigma_u^+:\Delta R = 0$ curves. Langevin and Langevin/4 are also plotted for comparison.

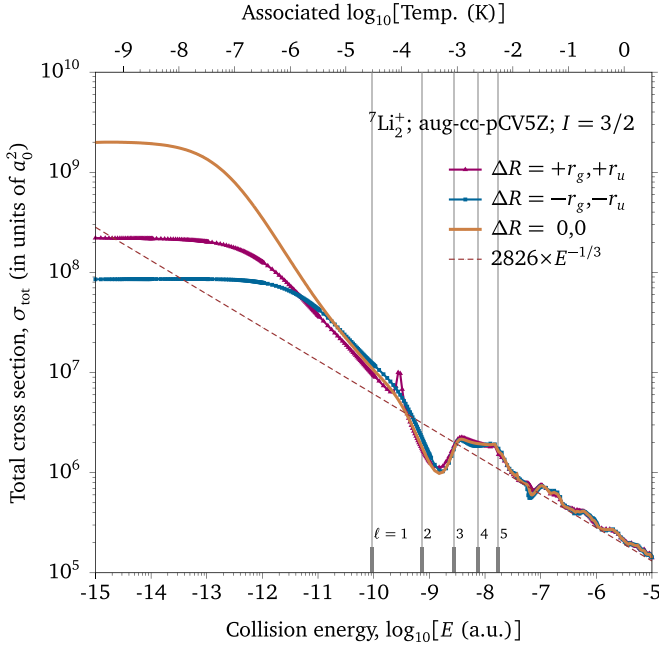


FIG. 7. Total collision cross sections, $\sigma_{\text{tot}}(E)$, of the ${}^7\text{Li}^+ - {}^7\text{Li}$ system in its first asymptotic state, which involves the electronic states $X^2\Sigma_g^+$ and $A^2\Sigma_u^+$, for the modified PECs $X/A:\Delta R = \pm(r_g, r_u)$ and $X/A:\Delta R = 0, 0$. The semiclassical cross section, $2826 \times E^{-1/3}$, and the centrifugal barrier energies for $\ell = 1-5$ are also shown.

significantly in the s -wave limit from the value calculated as the average of $S_g(E)$ and $S_u(E)$. For ${}^7\text{Li}^+ - {}^7\text{Li}$, in the s -wave limit, the cross section obtained using $\sigma_{\text{tot}}(E)$ is 25% smaller than the average of $S_g(E)$ and $S_u(E)$. The total cross section, $\sigma_{\text{tot}}(E)$, for ${}^7\text{Li}^+ - {}^7\text{Li}$ is plotted along with the semiclassical scattering cross section, $\sigma_{\text{sc}}(E)$, in Fig. 7. The centrifugal barrier energies introduced by the first few partial waves are also shown.

The scattering length a_u , when compared with the characteristic interaction length scale R^* , i.e., the position of the $\ell = 1$ barrier $(\alpha_d \times \mu/\hbar^2)^{1/2}$, which for ${}^7\text{Li}^+ - {}^7\text{Li}$ is $1024a_0$, is within a factor of 2, while a_g is very large (see Table IV). Also, $S_g(E)$ and a_g are more sensitive to the small- R region of the PEC and, consequently, to the details of the short-range interaction than $S_u(E)$ and a_u . This sensitivity of $X^2\Sigma_g^+$ is amplified for the ${}^7\text{Li}^+ - {}^7\text{Li}$ system, which is also noted by Schmid *et al.* [28], due to the proximity of a scattering pole,

TABLE IV. ${}^7\text{Li}^+ - {}^7\text{Li}$ scattering lengths for the modeled $X^2\Sigma_g^+:\Delta R = \pm r_g$, $X^2\Sigma_g^+:\Delta R = 0$ and $A^2\Sigma_u^+:\Delta R = \pm r_u$, $A^2\Sigma_u^+:\Delta R = 0$ curves are listed. For direct comparison with Zhang *et al.* [27] and Schmid *et al.* [28], the values obtained from $X/A:\Delta R = 0$ are appropriate.

$X^2\Sigma_g^+$, $A^2\Sigma_u^+$	$\Delta R = \pm r_{g,u}$	$\Delta R = 0$	[27]	[28]
a_g	-6582/3948	20 465	14 337	7 162
a_u	1432/1227	1 325	1 262	—

i.e., the PEC either is about to attain or has just attained a weakly bound state.

IV. DISCUSSION AND CONCLUSION

The values of D_e calculated by Zhang *et al.* [27] and Schmid *et al.* [28], along with the value calculated in this work (Table III), fall within the experimental accuracy of $10\,464 \pm 6 \text{ cm}^{-1}$ [47]. However, the convergence of E_e and E_∞ and the variational nature of the calculation provide additional certainty in our case. We have calculated the relativistic corrections using the second-order Douglas-Kroll-Hess Hamiltonian [36]. Relativistic corrections on the PECs can be expressed in two parts: a constant shift by $\approx -306.6 \text{ cm}^{-1}$ and an R -dependent change in the total electronic energy. The constant shift due to relativistic corrections does not affect the scattering calculations. The R -dependent change in the total electronic energy is less than 1.0 cm^{-1} for $R > R_e$ and less than 5.0 cm^{-1} for $R < R_e$, which is not significant compared with the effect of core electrons in the calculation, which is $\pm 140 \text{ cm}^{-1}$ at the repulsive wall position, R_{in} , for the allowed change of $\pm r_g$ in the $X^2\Sigma_g^+$ curve. We have found that the variation in the diagonal Born-Oppenheimer correction is less than 0.5 cm^{-1} over the entire internuclear range [52]. In addition, as we have discussed, counterpoise corrections for basis-set superposition error is not relevant in our case.

In the present work, an analysis is performed to obtain consistent asymptotic extensions of the scattering potentials. We find that the ${}^7\text{Li}^+ - {}^7\text{Li}$ system in the $X^2\Sigma_g^+$ state is close to a scattering pole, and therefore extreme care is required in the computation of low-energy scattering parameters. Scattering lengths for $X^2\Sigma_g^+:\Delta R = 0$ and $A^2\Sigma_u^+:\Delta R = 0$ are $20\,465a_0$ and $1325a_0$, respectively (see Table IV). The scattering lengths, a_g , reported by Zhang *et al.* [27] and Schmid *et al.* [28] are $14\,337a_0$ and $7162a_0$, respectively. Schmid *et al.* also provide a bound on a_g of $(107\,825a_0, 3664a_0)$, which corresponds to the potentials scaled by $(0.999, 1.001)$ to the computed PEC. The possible errors in the cross section, in our case, are estimated by controlled variations in the small- R region of the PECs, assessing the change they bring to the phase shifts and cross sections in the low-energy limit. The scattering pole for $X^2\Sigma_g^+$ occurs within the determined range of variations as shown in Fig. 3, particularly between the PEC models $\Delta R = +r_g$ and $\Delta R = 0$; this is also evident in the phase shift plot (Fig. 5), which prevents us from estimating the upper limit of the total cross section. However, the lower limit of the total cross section is given by the $\Delta R = -r_g, -r_u$ curve. The setting of this range will prevent the values reported here from being affected by even more sophisticated calculations in the future. The calculated value of the total cross sections is shown by the $\Delta R = 0$ curve in Fig. 7. The cross sections are determined for a wide range of collision energies, from 10^{-5} to 10^{-15} a.u., which covers a large range of temperatures, from a few K to a few nK. $S_g(E)$, $S_u(E)$, $S_{\text{ce}}(E)$, and $\sigma_{\text{tot}}(E)$ in the temperature regimes below a few mK have contributions from only a few partial waves (about five). In this regime, the cross sections significantly deviate from the semiclassical values and result in the distinctive features that can be explored in future experiments. The total cross section for the ${}^7\text{Li}^+ - {}^7\text{Li}$ system in the low-energy limit is $(1.9 \times 10^9)a_0^2$. When the

collision energy is higher than a few mK, many partial waves participate in the scattering and their contributions sum up to give the semiclassical value.

ACKNOWLEDGMENT

The authors acknowledge support from IFC-PAR/CEFIPRA Grant No. 5404-1.

- [1] A. T. Grier, M. Cetina, F. Oručević, and V. Vuletić, *Phys. Rev. Lett.* **102**, 223201 (2009).
- [2] C. Zipkes, S. Palzer, C. Sias, and M. Köhl, *Nature* **464**, 388 (2010).
- [3] S. Schmid, A. Härter, and J. H. Denschlag, *Phys. Rev. Lett.* **105**, 133202 (2010).
- [4] Z. Meir, T. Sikorsky, R. Ben-Shlomi, N. Akerman, Y. Dallal, and R. Ozeri, *Phys. Rev. Lett.* **117**, 243401 (2016).
- [5] L. Ratschbacher, C. Zipkes, C. Sias, and M. Köhl, *Nat. Phys.* **8**, 649 (2012).
- [6] S. Haze, S. Hata, M. Fujinaga, and T. Mukaiyama, *Phys. Rev. A* **87**, 052715 (2013).
- [7] S. Haze, R. Saito, M. Fujinaga, and T. Mukaiyama, *Phys. Rev. A* **91**, 032709 (2015).
- [8] K. Ravi, S. Lee, A. Sharma, G. Werth, and S. Rangwala, *Nat. Commun.* **3**, 1126 (2012).
- [9] I. Sivarajah, D. Goodman, J. Wells, F. Narducci, and W. W. Smith, *Phys. Rev. A* **86**, 063419 (2012).
- [10] S. Dutta, R. Sawant, and S. A. Rangwala, *Phys. Rev. Lett.* **118**, 113401 (2017).
- [11] F. H. J. Hall, M. Aymar, N. Bouloufa-Maafa, O. Dulieu, and S. Willitsch, *Phys. Rev. Lett.* **107**, 243202 (2011).
- [12] S. J. Schowalter, A. J. Dunning, K. Chen, P. Puri, C. Schneider, and E. R. Hudson, *Nat. Commun.* **7**, 12448 (2016).
- [13] A. Härter, A. Krüchow, A. Brunner, W. Schnitzler, S. Schmid, and J. H. Denschlag, *Phys. Rev. Lett.* **109**, 123201 (2012).
- [14] M. Morita, T. Sikorsky, Z. Meir, A. Buchachenko, R. Ben-Shlomi, N. Akerman, E. Narevicius, T. V. Tscherebul, and R. Ozeri, *Bull. Am. Phys. Soc.* **63**, H08.005 (2018).
- [15] T. Sikorsky, Z. Meir, R. Ben-Shlomi, N. Akerman, and R. Ozeri, *Nat. Commun.* **9**, 920 (2018).
- [16] L. Wang, M. Deiß, G. Raithel, and J. H. Denschlag, [arXiv:1901.08781](https://arxiv.org/abs/1901.08781).
- [17] H. Massey, *Contemp. Phys.* **13**, 135 (1972).
- [18] M. Cetina, A. T. Grier, and V. Vuletić, *Phys. Rev. Lett.* **109**, 253201 (2012).
- [19] T. Feldker, H. Fürst, H. Hirzler, N. Ewald, M. Mazzanti, D. Wiater, M. Tomza, and R. Gerritsma, *Nat. Phys.* **16**, 413 (2020).
- [20] R. Ben-Shlomi, R. Vexiau, Z. Meir, T. Sikorsky, N. Akerman, M. Pinkas, O. Dulieu, and R. Ozeri, [arXiv:1907.06736](https://arxiv.org/abs/1907.06736).
- [21] A. Härter and J. Hecker Denschlag, *Contemp. Phys.* **55**, 33 (2014).
- [22] J. Joger, H. Fürst, N. Ewald, T. Feldker, M. Tomza, and R. Gerritsma, *Phys. Rev. A* **96**, 030703(R) (2017).
- [23] R. Côté, *Phys. Rev. Lett.* **85**, 5316 (2000).
- [24] R. Côté and A. Dalgarno, *Phys. Rev. A* **62**, 012709 (2000).
- [25] S. Lee, K. Ravi, and S. A. Rangwala, *Phys. Rev. A* **87**, 052701 (2013).
- [26] S. Dutta and S. Rangwala, *Phys. Rev. A* **97**, 041401 (2018).
- [27] P. Zhang, E. Bodo, and A. Dalgarno, *J. Phys. Chem. A* **113**, 15085 (2009).
- [28] T. Schmid, C. Veit, N. Zuber, R. Löw, T. Pfau, M. Tarana, and M. Tomza, *Phys. Rev. Lett.* **120**, 153401 (2018).
- [29] I. Schmidt-Mink, W. Müller, and W. Meyer, *Chem. Phys.* **92**, 263 (1985).
- [30] S. Magnier, S. Rousseau, A. Allouche, G. Hadinger, and M. Aubert-Frécon, *Chem. Phys.* **246**, 57 (1999).
- [31] H. Bouzouita, C. Ghanmi, and H. Berriche, *J. Mol. Struct. THEOCHEM* **777**, 75 (2006).
- [32] P. Jasik, J. Wilczyński, and J. Sienkiewicz, *Eur. Phys. J.-Spec. Top.* **144**, 85 (2007).
- [33] M. Musiał, M. Medrek, and S. A. Kucharski, *Mol. Phys.* **113**, 2943 (2015).
- [34] D. Rabli and R. McCarroll, *Chem. Phys.* **487**, 23 (2017).
- [35] S. Nasiri and M. Zahedi, *Comput. Theor. Chem.* **1114**, 106 (2017).
- [36] H.-J. Werner, P. J. Knowles, G. Knizia, F. R. Manby, and M. Schütz, *WIREs Comput. Mol. Sci.* **2**, 242 (2012).
- [37] H.-J. Werner and P. J. Knowles, *J. Chem. Phys.* **89**, 5803 (1988).
- [38] B. P. Prascher, D. E. Woon, K. A. Peterson, T. H. Dunning, and A. K. Wilson, *Theoret. Chem. Accounts* **128**, 69 (2011).
- [39] G. W. Drake, *Springer Handbook of Atomic, Molecular, and Optical Physics* (Springer Science & Business Media, Berlin, 2006).
- [40] Z.-C. Yan and G. W. Drake, *Phys. Rev. A* **52**, 3711 (1995).
- [41] See Supplemental Material at <http://link.aps.org/supplemental/10.1103/PhysRevA.101.052702> for *ab initio* MRCI calculation with aug-cc-pCV5Z basis set. The primary calculation is performed with $0.2a_0$ step size for the range $[2a_0 - 50a_0]$. The step size for R of PECs provided in the supplementary is $0.01a_0$. In the scattering calculation, the smallest step size used is $0.001a_0$. We have checked the consistency of results with many intermediate step-sizes, and we find that the used step size is adequate. Also, the scattering PECs provided are up to $1000a_0$ only. In the scattering calculation, computation range of PEC is determined by the condition $R = 10\lambda$ when $\lambda > 100a_0$, and $R = 1000a_0$ when $\lambda < 100a_0$ where λ is the de Broglie wavelength of the system. For the collision energy range used in the paper, 10^{-5} a.u. $> E > 10^{-15}$ a.u., for ${}^7\text{Li}^+ - {}^7\text{Li}$, the range of λ is $10a_0 < \lambda < 10^6a_0$. The condition and range are discussed in the Secs. II B and III.
- [42] M. Aymar and O. Dulieu, *J. Chem. Phys.* **122**, 204302 (2005).
- [43] R. Côté, in *Advances in Atomic, Molecular, and Optical Physics*, edited by E. Arimondo, C. C. Lin, and S. F. Yelin (Academic Press, San Diego, CA, 2016), Vol. 65, pp. 67–126.
- [44] L.-Y. Tang, Z.-C. Yan, T.-Y. Shi, and J. F. Babb, *Phys. Rev. A* **79**, 062712 (2009).
- [45] J. Mitroy, M. S. Safronova, and C. W. Clark, *J. Phys. B* **43**, 202001 (2010).

- [46] J. Bardsley, T. Holstein, B. Junker, and S. Sinha, *Phys. Rev. A* **11**, 1911 (1975).
- [47] R. Bernheim, L. Gold, T. Tipton, and D. Konowalow, *Chem. Phys. Lett.* **105**, 201 (1984).
- [48] R. Bernheim, L. Gold, and T. Tipton, *J. Chem. Phys.* **78**, 3635 (1983).
- [49] R. J. Le Roy, *J. Quant. Spectrosc. Radiat. Transfer* **186**, 167 (2017).
- [50] J. K. Watson, *J. Mol. Spectrosc.* **80**, 411 (1980).
- [51] N. Joshi *et al.* (unpublished).
- [52] J. J. Lutz and J. M. Hutson, *J. Mol. Spectrosc.* **330**, 43 (2016).